

We are IntechOpen, the world's leading publisher of Open Access books Built by scientists, for scientists

6,900

Open access books available

186,000

International authors and editors

200M

Downloads

Our authors are among the

154

Countries delivered to

TOP 1%

most cited scientists

12.2%

Contributors from top 500 universities



WEB OF SCIENCE™

Selection of our books indexed in the Book Citation Index
in Web of Science™ Core Collection (BKCI)

Interested in publishing with us?
Contact book.department@intechopen.com

Numbers displayed above are based on latest data collected.
For more information visit www.intechopen.com



Lipid Self-Spreading on Solid Substrates

Irep Gözen, Paul Dommersnes and Aldo Jesorka

Additional information is available at the end of the chapter

<http://dx.doi.org/10.5772/61584>

Abstract

This chapter is dedicated to wetting and fracturing processes involving molecular phospholipid films and high-energy solid surfaces. In these systems, wetting of planar surfaces occurs in an aqueous environment by means of self-spreading of phospholipid membranes from artificially generated lipid sources, which range from manually deposited single sources (multilamellar liposomes) to liposome suspensions of different particle sizes, which are directly pipetted onto the substrate. The most prominent of the molecular lipid films is the phospholipid bilayer, which constitutes the fundamental structure of the biological cell membrane. Lipid membranes have peculiar characteristics, are highly dynamic, feature two-dimensional fluidity, and can accommodate functional molecules. Understanding the interactions of lipid films with solid interfaces is of high importance in areas like cell biology, biomedical engineering, and drug delivery.

Keywords: Phospholipid bilayer, phospholipid double bilayer, phospholipid monolayer, supported bilayer, lipid self-spreading

1. Introduction

This chapter highlights recent advances in wetting of solid surfaces by the self-spreading of phospholipid biomembranes upon deposition of lipid reservoirs [1, 2]. It should provide researchers with the necessary material to understand and evaluate spontaneous propagation of lipid monolayers [2, 3] and double bilayers [2, 4] on solid supports, which occurs when lipid reservoirs are brought in contact with low- and high-energy surfaces, respectively, in an aqueous environment. The first section provides a brief introduction of surfaces and interfaces, the second section is dedicated to the mechanism of interaction of lipid films with the sup-

porting surface during wetting, and the third section introduces the formation of ruptures in double bilayers caused by that interaction.

Biological membranes organize cellular complexity, and thus establish and promote structure in the living world [5]. They compartmentalize the cell, form transport networks, organize proteins, serve as a smart barrier for molecules and ions, and establish the chemical identity of the cell. The fundamental structure of the cellular membrane is the phospholipid bilayer, consisting of a large number of individual phospholipid molecules, which organize themselves spontaneously in a self-assembly process. The membrane has peculiar characteristics, is highly dynamic, and features two-dimensional fluidity [6]. It can accommodate proteins and other functional molecules which fulfil important functions such as recognition, signal transduction, and transport of chemical entities through the membrane.

Biomembrane models, designed to capture some of the features of the cell membrane in a simplified setting, have become a popular research subject [7, 8]. They are naturally less complex than their biological counterpart, but can be relatively easily assembled, for example, on suitable flat solid surfaces (supported membranes), or as spherical membrane compartments, often referred to as vesicles or liposomes [9]. In the past few decades, a large number of model systems of increasing sophistication have been introduced, often with the purpose to identify and study the role and function of lipids and other membrane components in the cell [7, 10]. In particular, the two-dimensional fluidity of the membrane and their ability to harbour proteins have been in the centre of attention.

Although self-organization of lipid molecules to lipid membranes occurs spontaneously, which is frequently exploited to assemble membranes from lipid mixtures in solution in experimental settings, controlled assembly and preparation of stable, well-defined phospholipid films on supporting surfaces, such as glass, metals and metal oxides, are still challenging engineering tasks.

The deposition of lipid reservoirs onto various solid surfaces leads to formation of self-spreading surface-supported lipid films [1, 11]. Lipid reservoirs range from manually deposited single sources (multilamellar liposomes) to liposome suspensions of different particle sizes [10, 12], which can be directly transferred onto the substrate, either manually with glass microneedles [13] or by means of sophisticated microfluidic instrumentation [10, 14]. The following chapter is dedicated to the formation of lipid mono- and bilayer membranes by means of self-spreading from a lipid source. The result of lipid spreading is typically a solid-supported self-assembled membrane, i.e., a continuous supramolecular structure with two-dimensional fluidity. Each of the three forms of supported membranes mentioned above represents a real biological structure. Monolayers surround lipid droplets in cells, which are small stocks of lipid molecules regulating lipid metabolism of the cell [15]. Single bilayers are – in terms of composition – simplified versions of the plasma membrane of cells, which resides on top of the cytoskeleton. Spreading double bilayers are reminiscent of spreading cell membranes, which in addition to a lipid membrane contain actin filaments [16]. Accordingly, each of the supported membrane types can be utilized in experimental studies to address different questions. The supported bilayer is the most commonly used model system, as it directly resembles the membrane of the biological cell. Supported bilayer structures can be

easily prepared in an aqueous environment on available surfaces that are compatible with microscopy experiments, such as glass, mica, or sapphire plates. Nowadays, with microfabrication and micromanipulation equipment being commonplace, a greater variety of surfaces is available, for example, silicon or aluminium oxide coated glass, which opened pathways for the generation of self-spreading double bilayers from lipid reservoirs. In particular, amorphous fluoropolymers and the epoxy photoresist SU-8, which can be utilized to coat and pattern a variety of surfaces with nanoscopic polymer films [17, 18], have enabled experiments where single reservoirs are manually deposited, allowing for the controlled generation of self-spreading lipid monolayers. Table 1 gives an overview over the most relevant publications [19 - 54] in the area of lipid film research from 1985 to present. It covers fabrication, biophysical characterization, and utilization in, for example, membrane protein studies.

	Article title	Authors	Source title	Year	Reference	Key points
1	<i>Wetting: Statics and dynamics</i>	De Gennes, P.G.	Rev. Modern Phys.	1985	[19]	One of the first articles in wetting of liquids on solid substrates, cited 3700 times
2	<i>Translational and rotational drag coefficients for a disk moving in a liquid membrane associated with a rigid substrate.</i>	Evans E. And Sackmann S.	Journal of Fluid Mechanics	1988	[20]	First theoretical framework of spreading/wetting membranes and relation to friction (drag) coefficient; supports the current model explained throughout the chapter.
3	<i>Phenomenology and kinetics of lipid bilayer spreading on hydrophilic surfaces.</i>	Rädler J. et al.	Langmuir	1995	[2]	Pioneer study, kinetics of lipid wetting via self-spreading lipid reservoirs: bilayer, double bilayer membranes
4	<i>Supported membranes: scientific and practical applications.</i>	Sackmann, E.	Science	1996	[8]	First examples of polymer cushioned protein incorporated bilayers, double bilayers, supported lipid bilayer-based biosensors
5	<i>Wetting films of lipids in the development of sensitive interfaces. An electrochemical approach.</i>	Kochev V. And Karabaliev M.	Advances in Colloid and Interface Science	2004	[21]	Review of basic principles underlying the techniques of formation, as well as the conditions of the films stability.
6	<i>Growth of giant membrane lobes mechanically driven by wetting fronts of phospholipid membranes at water-solid interfaces.</i>	Suzuki K. and Masuhara H.	Langmuir	2005	[22]	Multilayer self-spreading lipid bilayers

	Article title	Authors	Source title	Year	Reference	Key points
7	<i>Wetting fibers with liposomes.</i>	Borghi N. <i>et al.</i>	J. of Colloid and Interface Sci.	2005	[23]	Coating fibers with lipids through lipid wetting
8	<i>Following the formation of supported lipid bilayers on mica: A study combining Afm, Qcm-D, and ellipsometry.</i>	Richter R.P. <i>et al.</i>	Biophysical Journal	2005	[24]	Study of bilayer formation dynamics by a combination approach of different analytical surface techniques
9	<i>On the kinetics of adsorption and two-dimensional self-assembly of annexin A5 on supported lipid bilayers.</i>	Richter R.P. <i>et al.</i>	Biophysical Journal	2005	[25]	Supported membrane protein studies
10	<i>Formation of solid-supported lipid bilayers: An integrated view.</i>	Richter R.P. <i>et al.</i>	Langmuir	2006	[26]	Study of bilayer formation dynamics
11	<i>Supported lipid bilayer self-spreading on a nanostructured silicon surface.</i>	Furukawa K. <i>et al.</i>	Langmuir	2006	[27]	Self-spreading in combination with nanostructured surfaces
12	<i>Direct immobilization of cholesteryl-TEG-modified oligonucleotides onto hydrophobic SU-8 surfaces.</i>	Erkan Y. <i>et al.</i>	Langmuir	2007	[28]	Lipid monolayer self-spreading/wetting
13	<i>Controlled formation and mixing of two-dimensional fluids.</i>	Czolkos I. <i>et al.</i>	Nano Letters	2007	[3]	Lipid monolayer self-spreading/wetting
14	<i>Supported lipid bilayer/ carbon nanotube hybrids.</i>	Zhou X. <i>et al.</i>	Nature Comm.	2007	[29]	Lipid wetting over single-walled carbon nanotube transistors
15	<i>Membrane lipids: where they are and how they behave.</i>	Van Meer G. <i>et al.</i>	Nature Rev. Mol. Cell Biol.	2008	[30]	Review on plasma membrane lipids: structure, phase behavior, function
16	<i>Plasma membrane area increases with spread area by exocytosis of a GPI-anchored protein compartment.</i>	Gauthier N.C. <i>et al.</i>	Mol. Biology of the Cell	2009	[31]	Cell membrane spreading similar to double lipid bilayer spreading
17	<i>Protrusive growth and periodic contractile motion in surface-adhered vesicles induced by Ca^{2+}-gradients.</i>	Lobovkina T. <i>et al.</i>	Soft Matter	2010	[11]	Double lipid bilayer self-spreading/localized Marangoni flow

Article title	Authors	Source title	Year	Reference	Key points
18 <i>Fractal avalanche Ruptures in biological membranes</i>	Gözen I. et al.	Nature Materials	2010	[4]	Double lipid bilayer self-spreading, wetting through rupturing
19 <i>Quartz crystal microbalance with dissipation monitoring of supported lipid bilayers on various substrates</i>	Cho N.J. et al.	Nature Protocols	2010	[32]	QCM-D as a measure of wetting of solid surfaces by lipid bilayers
20 <i>Changes in wetting and energetic properties of glass caused by deposition of different lipid layers.</i>	Gołabek M., Hołysz L.	Applied Surface Science	2010	[33]	Investigation of wetting and energetic properties of different lipid layers deposited on the glass surface, carried out by contact angles measurements and determination of the apparent surface free energy .
21 <i>A Self-assembly route for double bilayer lipid membrane formation</i>	Han X. et al.	ChemPhysChem	2010	[34]	Bilayer on bilayer formation using fusogenic reagents
22 <i>Evolution of supported planar lipid bilayers on step-controlled sapphire surfaces</i>	Isono T., Ikeda T., and Ogino T.	Langmuir	2010	[35]	Supported bilayer wetting on varying topology
23 <i>Templating membrane assembly, structure, and dynamics using engineered interfaces</i>	Oliver A.E. and Parikh A.N.	Biochim. Biophys. Acta - Biomembranes	2010	[36]	Monolayer/bilayer/interfaces
24 <i>Calcium-ion-controlled nanoparticle-induced tubulation in supported flat phospholipid vesicles</i>	Gözen I. et al.	Soft Matter	2011	[37]	Lipid wetting is tuned with Ca ²⁺ ions, leading to tubulation
25 <i>Control of dynamics and molecular distribution in a self-spreading lipid bilayer using surface-modified metal nanoarchitectures.</i>	Nabika H. et al.	Phys. Chem. Chem. Phys.	2011	[38]	Self-spreading bilayers on nanostructures
26 <i>Using patterned supported lipid membranes to investigate the role of receptor organization in intercellular signaling</i>	Nair P.M. et al.	Nature Protocols	2011	[39]	Protocol supported bilayer, SUV rupture

Article title	Authors	Source title	Year	Reference	Key points
27 <i>Mechanism of lipid nanodrop spreading in a case of asymmetric wetting.</i>	Mohamad, S. <i>et al.</i>	Physical Review Letters	2012	[40]	Involves surface-enhanced ellipsometric contrast microscopy to observe the spreading of egg phosphatidylcholine nanodroplets on a hydrophilic substrate
28 <i>Instrumental methods to characterize molecular phospholipid films on solid supports</i>	Gözen I. and Jesorka A.	Analytical Chemistry	2012	[41]	Review on characterization methods and tools for surface-supported membranes
29 <i>Evidence for membrane flow through pores in stacked phospholipid membranes</i>	Gozen I. <i>et al.</i>	Soft Matter	2012	[42]	Wetting of proximal bilayers via rupturing of distal bilayers
30 <i>Mechanical feedback between membrane tension and dynamics</i>	Gauthier N.C. <i>et al.</i>	Trends in Cell Biology	2012	[43]	Cell spreading
31 <i>Glycans pattern the phase behaviour of lipid membrane.</i>	Subramaniam A.B. <i>et al.</i>	Nature Materials	2013	[44]	How self-spreading model membranes can be used to understand membrane-mediated transport processes. Findings indicate an intimate coupling between cellular lipidomes and glycomes.
32 <i>Multiplexed biomimetic lipid membranes on graphene by dip-pen nanolithography</i>	Hirtz M. <i>et al.</i>	Nature Comm.	2013	[45]	Lipid bi-/multilayer wetting using dip-pen lithography
33 <i>Repair of large area pores in supported double bilayers</i>	Gözen I. <i>et al.</i>	Soft Matter	2013	[46]	Different cause of bilayer-on-bilayer wetting
34 <i>Mechanics of spreading cells probed by atomic force microscopy</i>	Pietuch A., and Janshoff A.	Open Biology	2013	[47]	Cell spreading
35 <i>Lab on a Biomembrane: Rapid prototyping and manipulation of 2D fluidic lipid bilayer circuits</i>	Ainla A. <i>et al.</i>	Scientific Reports	2013	[10]	Printed/spreading bilayers deposited by a microfluidic pipette
36 <i>Spatial organization of cytokinesis</i>	Nguyen P.A. <i>et al.</i>	Science	2014	[48]	Supported bilayers used to study the effect of (artificial)

Article title	Authors	Source title	Year	Reference	Key points
<i>signaling reconstituted in a cell-free system</i>					centrosomes, an application example
37 <i>Effective Brownian ratchet separation by a combination of molecular filtering and a self-spreading lipid bilayer system.</i>	Motegi T. <i>et al.</i>	Langmuir	2014	[49]	Nanofabricated obstacle-based molecular filtering of self-spreading lipid bilayer membrane
38 <i>Arrayed lipid bilayer chambers allow single-molecule analysis of membrane transporter activity</i>	Watanabe R. <i>et al.</i>	Nature Comm.	2014	[50]	Lipid wetting from a lipid reservoir, this time not onion-like but dissolved lipids in solvent used for single-molecule studies
39 <i>Solvent-assisted lipid bilayer formation on silicon dioxide and gold</i>	Tabaei S. <i>et al.</i>	Langmuir	2014	[51]	Impact of solvent in membrane wetting type
40 <i>Nanopatterning of mobile lipid monolayers on electron-beam-sculpted teflon AF surfaces</i>	Shaali M. <i>et al.</i>	ACS Nano	2015	[52]	Precise patterning of self-spreading monolayers using E-beam lithography
41 <i>Discovery of the migrasome, an organelle mediating release of cytoplasmic contents during cell migration</i>	Ma L. <i>et al.</i>	Cell Research	2015	[53]	Plasma membrane dewetting on solid support during cell migration
42 <i>A versatile nano display platform from bacterial spore coat proteins</i>	Wu, I.-L. <i>et al.</i>	Nature Comm.	2015	[[54]]	Solid support as micron-size silica beads (spherical) instead of flat surfaces

Table 1. Selected publications in the field of lipid self-spreading/wetting

2. Surfaces and interfaces

Supported lipid membranes form on solid surfaces, where many of the membrane properties are depending on the properties of the underlying surface, including material and composition, surface charge, roughness, and surface tension. The wetting phenomena observed in double bilayers only occur on solid high-energy surfaces, such as silicon oxide, or aluminium oxide films. In contrast, the wetting phenomena leading to lipid monolayers occur exclusively on low-energy hydrophobic polymer surfaces. The surface tension is a central concept, that is, in principle, a measure of how much energy is associated with a surface per unit area. If in a thought experiment a cube with the side length a , consisting of a solid material, is split into

two parts of identical size, work of cohesion W must be exerted, equal to the difference in free energy $G_2 - G_1$, which characterize the system before and after the split. If $A = a^2$ is the area of the separation, then $F = W/A$ is the surface free energy of the newly created surfaces. The surface tension σ of the material can be defined, which is a measure of how much work is required to create a surface of area A [55]:

$$\sigma = F + A \frac{\partial F}{\partial A} \quad (1)$$

High-energy surfaces ($\sigma > 500 \text{ Nm/m}$) are composed of atoms which are attached to each other by covalent, ionic, or metallic bonds. Examples include metals, diamond, silica, glasses, and ceramics. Molecules of low-energy surfaces, such as various polymers, are attached to each other by the weaker van der Waals interactions or hydrogen bonds. It is evident that the intermolecular forces which determine the surface energy of a material also determine latent heat, melting, and boiling point. Materials with high boiling points ($T > 2000^\circ\text{C}$) usually also have high-surface energies.

In water (and likewise in other monomolecular fluids), the molecules in the bulk are surrounded by other water molecules, where they are energetically indistinguishable. Only at solid and gas interfaces (e.g., the walls of a container, or the water vapour/water interface in an open container), there are molecules which experience different forces. The resulting energetic differences with respect to the bulk molecules are reflected by the interfacial tension of the solid–liquid interface σ_{SL} , and the surface tension of the liquid σ_{LV} at the liquid–vapour interface. Accordingly, the surface tension of a solid in equilibrium with a liquids vapour is σ_{SV} . A typical value of σ_{LV} for water is 73 mN/m [56, 57]. Temperature increase and added solutes lead to a noticeable decrease in surface tension. At a contact line between liquid, solid, and fluid at equilibrium (e.g., a fluid droplet in saturated air on a planar surface), the three interfacial tensions are force-balanced. The Young equation describes this force balance, and introduces a contact angle ϑ between the fluid/vapour and fluid/solid interface as a convenient measure of surface hydrophobicity/hydrophilicity:

$$\sigma_{SV} - \sigma_{SL} = \sigma_{LV} \cos \vartheta \quad (2)$$

Hydrophobic (or high-energy) surfaces feature small contact angles of $\vartheta < 90^\circ$, since the system is minimizing its free energy by spreading the droplet across the surface. The dynamics of wetting and spreading of fluids on solid surfaces have been extensively reviewed in other publications [58] and will not be further discussed here. However, the Young equation allows only direct observation of σ_{LV} and ϑ . Direct comparison of solid surfaces by means of their surface tensions is not possible, since these values cannot be obtained in a straightforward manner. By introducing the concept of a critical surface tension σ_c , at which complete wetting occurs ($\cos \vartheta = 1$), solids can be well compared with respect to their wetting behaviour. Materials with strong cohesion, such as oxides and metals, can be categorized under high

critical surface tension materials ($\sigma_c \gg 100$ mN/m), whereas polymers and other organic films typically feature low critical surface tensions ($\sigma_c < 50$ mN/m). The nature of lipid films formed on such surfaces depends very much on the surface energy.

In addition, the roughness of a surface is of considerable importance to its wetting properties, which was discovered by Wenzel in 1936 [59]. In nature, topographical surfaces with regular or irregular features on the micro- or nanoscale have a water-repelling function. The most prominent examples are the leaves of the Sacred Lotus, which has a nanopatterned surface to protect it from water, and the skin of sharks, which give the animal the ability to move faster in water. These superhydrophobic surface features, which are characterized by very large contact angles of $\vartheta > 150^\circ$, cannot be described by the Young equation, but by the Cassie-Baxter surface model [59]. According to that model, which is applicable to extreme surface texture, water droplets cannot wet the surface, since they are forced to remain on top of the structures. The prominent topographical features prevent wettings, because the surface would have to bend down into the gaps, which would result in high local curvatures and high Laplace pressures, but also in an increased surface-to-volume ratio. Both surface energy and roughness have an influence on the wetting properties of lipid material when it comes in contact with the surface. For example, fluorocarbon films, generated by plasma decomposition and deposition of perfluorinated hydrocarbons, are more hydrophobic than epoxy polymer films, but their greater roughness makes them comparatively less suitable for large area spreading of lipid monolayers [60].

3. Lipid self-spreading

A lipid reservoir brought into contact with a solid substrate leads to wetting of the surface by lipids in the form of a molecularly thin phospholipid film. Lipid reservoirs can be considered as stocks of phospholipid molecules and can exist in various forms. Rädler et al. have used “solid lipid sources” as reservoirs, which they have described as irregularly wrapped (entangled) layers of lipid bilayers [2]. The reservoirs have been referred to as “lipid lumps” in a few other studies and illustrated as liquid drops in which the individual lipid molecules are randomly oriented [22]. Multilamellar vesicles (MLVs) containing several hundreds of lipid bilayers packed in a compact sphere can also be employed as lipid reservoirs [4, 11]. Because of their dense, layered structure, such vesicles are also referred to as “onion shell vesicles” [61]. The internal molecular structure of such lipid reservoirs can be complex and the mechanisms of initiation of wetting from such reservoirs have not yet been fully understood. We will further comment on the potential impact of the lipid reservoir structure on wetting dynamics in the later paragraphs of this chapter.

Due to wetting, individual lipids originating from a lipid source self-assemble on a solid surface as a planar lipid film, extending the surface area over a distance of several tens to hundreds of microns. The wetting motion of lipids on solid substrates is therefore commonly referred to as “lipid spreading”. Since the spreading is generally not initiated due to an external

stimulus, but begins rather spontaneously, ensuring energetically the most favourable conditions, the spreading is further defined as “lipid self-spreading”.

In context of this chapter, lipid wetting of a solid substrate occurs in biologically relevant conditions, e.g., in water-based physiological buffers. Let us consider the spreading of a lipid monolayer. When a lipid source is deposited on a hydrophobic substrate in the presence of an aqueous solution, surface tension at two interfaces may play a role in wetting. One is the tension at interface of lipids with the solid substrate (σ_L), the second is the tension at the interface of aqueous buffer (σ_A) with the solid substrate. In other words, the surface can be wetted by either phospholipids emerging from the lipid source or by the water molecules in the buffer. Lipid spreading will initiate spontaneously if the surface free energy of the system would be reduced during spreading. This is possible if σ_L is lower than σ_A . Accordingly, lipids would migrate from the lipid source to wet the substrate.

Structure of the wetting lipid film depends on the nature of the solid surface, e.g., if it is of high or low energy, a hydrophilic or hydrophobic substrate. Single bilayers tend to form on moderately hydrophilic substrates such as glass. Double bilayer wetting can be observed on silicon oxides and multiple metal oxide surfaces which are generally considered to be high-energy substrates. On hydrophobic surfaces like fluoropolymers or the epoxy SU-8, lipids spread as monolayers, i.e., as a single leaflet of a lipid bilayer. This can be expected since the hydrocarbon chains of lipid molecules would tend to face towards the hydrophobic surface.

The mechanism of interaction with the surface during wetting varies, depending on the nature of the substrate. The monolayer lipids form due to the hydrophobic interactions with the surface. Spreading monolayers screen along the buffer–surface interface, establishing a direct contact with the hydrophobic substrate (Figure 1a). During single bilayer spreading on glass or mica, there remains a thin (few nm) lubricating layer beneath the membrane (Figure 1b). The bilayers spread by “sliding” on top of the water layer. The interaction between the bilayer and the surface is governed by hydration and the van der Waals forces. Double bilayer spreading on highly oxidized silica or other metals is mostly under the influence of electrostatic interactions. Physiological buffers have high ionic strength and contain multivalent ions, for example, Ca^{2+} or Mg^{2+} . These positively charged entities in the ambient solution act as “fusogenic agents” and establish bridging connections between the negatively charged phospholipid headgroups and the negatively charged surface (Figure 1c). This facilitates the spreading of lipid films on oxidized surfaces. Concentrations of only a few mM/L [62] of divalent cations and 10^{-5} M of trivalent cations have a dramatic effect on surface potentials. For instance, they can neutralize a negatively charged surface and even start to accumulate positive charges [62]. A few studies have reported on multi-bilayer spreading featuring up to seven bilayers on Si/SiO₂ surfaces [22, 63], but very little is known about the spreading dynamics.

Self-spreading of multilamellar vesicles on solid substrates leads to circular lipid patches (Figure 1d). The main reason for the circular geometry lies in the spreading dynamics which is characterized by Darcy flow. Briefly, the spreading front can be described by the same equation that is used to describe a Saffman-Taylor instability (a specific form of Darcy flow), but with the opposite sign. Therefore, any perturbation from a circular shape during spreading

will be rapidly damped. We will explain thoroughly why membrane flow is a form of Darcy flow in the next section.

The overall tension (σ_s) during lipid wetting is expected to be:

$$\sigma_s = \sigma_A - \sigma_L \quad (3)$$

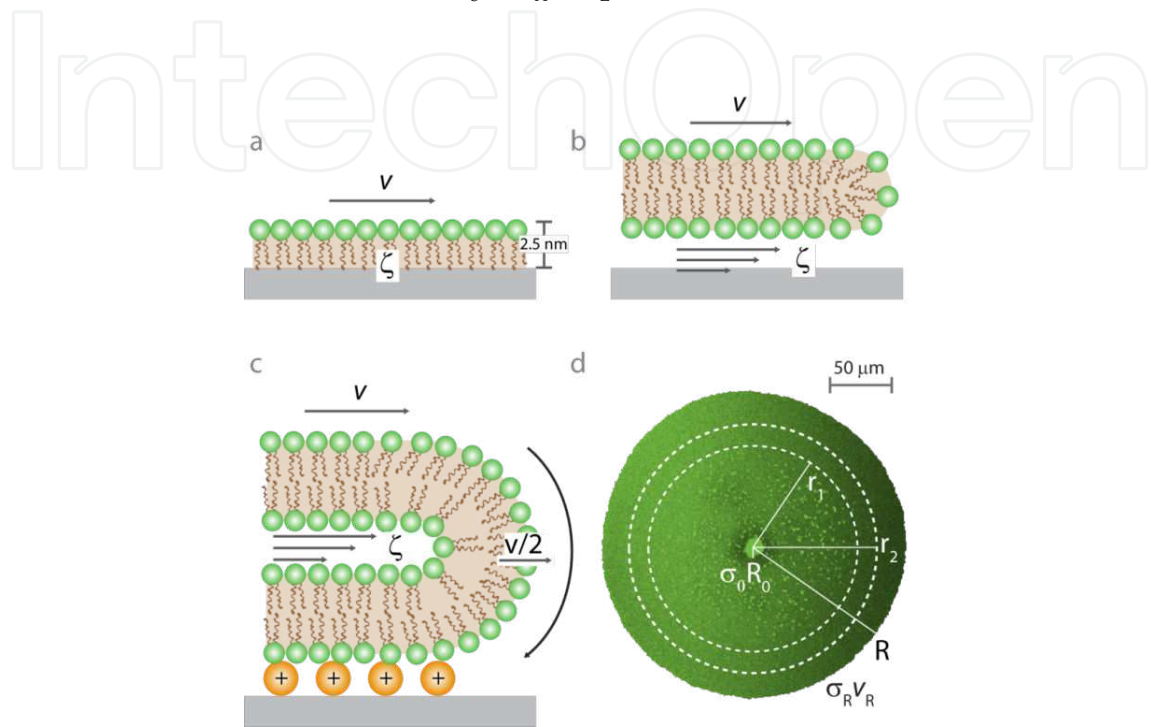


Figure 1. Lipid self-spreading. Illustrations showing in a side view the cross-sectional edge profiles of a spreading (a) monolayer, (b) single bilayer, and (c) double bilayer. The spreading monolayer is directly in contact with the substrate. The single bilayer exhibits sliding motion on a thin lubricating water layer. During double bilayer spreading, positively charged ions bridge the proximal (lower) bilayer to the surface, where the distal (upper) bilayer slides on a layer of water trapped in between the two layers. ζ indicates the region where the friction is effective during spreading. v is the velocity of the spreading membrane. (d) Laser scanning confocal micrograph of a self-spreading double bilayer (top view). The bright spot at the centre of the circular patch is the multilamellar lipid reservoir, from which lipid material is drawn.

Lipid self-spreading is therefore considered to be a form of *Marangoni flow*, which is the mass transfer between two fluids along an interface in a surface tension gradient. During spreading, there is mass transfer of lipids towards the buffer solution along the solid substrate.

The lipid reservoir has also an internal tension (σ_0) which will resist the spreading. The spreading power (S) can thus be formulated as the difference between overall interfacial tension and the tension of the reservoir:

$$S = \sigma_s - \sigma_0 = \sigma_A - \sigma_L - \sigma_0 \quad (4)$$

Note that the terms in Eq. (3) and (4) may not fully represent the single and the double bilayers. As described above, during monolayer spreading the lipids replace the water molecules on

the surface; therefore, terms σ_L and σ_A are appropriately describing the driving forces in lipid monolayer spreading. For the other two types of spreading, more complicated surface interactions may play a role. For instance, because of the existing lubricating water layer between the surface and the membrane during single and double bilayer spreading, the water molecules are not essentially replaced by lipids. Therefore, σ_S can simply be defined as the adhesion energy between the membrane and the surface, instead of the surface tension differences of σ_A and σ_L .

Different wetting modes of phospholipids can be distinguished by a kinetic spreading coefficient, β ; which is directly related to velocity (v) of the spreading membrane:

$$v(t) = \sqrt{\frac{\beta}{t}} \quad (5)$$

The spreading power (S), which quantifies the driving force for the spreading process, is composed of the spreading and the friction coefficients (ζ):

$$\beta = \frac{S}{2\zeta} \quad (6)$$

Next, we will formulate the spreading coefficients for different modes of lipid self-spreading on solid supports. These modes include monolayers, single bilayers, and double bilayers. We will first adapt a one-dimensional model which had been originally proposed by Rädler et al. for single lipid bilayer spreading [2].

We make two main assumptions to establish our model, which would be valid for all three types of lipid spreading:

- i. membrane flow can be described by a two-dimensional Stokes equation:

$$\zeta \bar{v} = \nabla \sigma - \mu \nabla^2 \bar{v} \quad (7)$$

where μ is the membrane viscosity (10^{-3} dyn s cm^{-1}) [64] and v is the membrane velocity. The first term describes the frictional forces and the second term the viscous shear forces. The viscous forces are only influential in membrane dynamics if the length of the membrane is below 30 nm. We will discuss in the next section in detail how the critical length (L_c), at which the impact of viscous forces is comparable to the frictional forces, has been determined. Since the lengths of the supported membranes are way above 30 nm, we now eliminate the second term in Eq. (7) and take into account only the first term:

$$\zeta \bar{v} = \nabla \sigma \Rightarrow \zeta v = \frac{d\sigma}{dx} \quad (8)$$

This means that the tension gradient ($\nabla \sigma$) which drives the spreading process is balanced by the frictional stress. For a monolayer or a single bilayer, ζ applies to the region between the surface and the lipid film. For a double bilayer membrane, ζ is effective between the proximal (lower) and the distal (upper) bilayers. This is due to the tank-thread-like motion of the double bilayer. In this type of motion, the proximal layer is immobilized as soon as it is fused to the surface via the multivalent ions and the distal bilayer slides over the proximal bilayer and lays onto the substrate. This is why the self-spreading double bilayer has been called by Rädler et al. “a rolling bilayer” [2].

ii. To a first degree of approximation, lipid membranes are incompressible [20].

$$\nabla \bar{v} = 0 \Rightarrow \frac{dv}{dx} = 0 \tag{9}$$

Combining Eq. (8) and (9) leads to:

$$\frac{d^2\sigma}{dx^2} = 0 \Rightarrow \sigma = ax + b \tag{10}$$

$\sigma(R) = \sigma_s$, where σ_s is the tension due to the adhesion to the surface. $\sigma(0) = \sigma_0$ is the tension of the lipid reservoir.

$$\sigma = \frac{\sigma_s - \sigma_0}{R} x + \sigma_0 \tag{11}$$

Combining Eq. (10) and (11) leads to:

$$\zeta v = \frac{\sigma_s - \sigma_0}{R} \text{ or } \zeta v R = \sigma_s - \sigma_0 \tag{12}$$

This means that the membrane flow caused by the tension difference over a radius R is dissipated by the friction. The velocity at the spreading edge of a double bilayer (v_R) will be half the velocity of the membrane (v) since the spreading edge exhibits rolling motion, where only half of the membrane material is laid upon the substrate. The membrane velocity of a monolayer or a single bilayer will be equal to the velocity at the spreading edge since such rolling motion is not performed. Because of this distinction among the spreading dynamics of different types of membranes, we will explain the model from this point on under two groups: (1) monolayer and single bilayers, (2) double bilayers. The equations for the calculation of β for group 1 will be denoted as “a” in the left column, and for group 2 as “b” for the right column.

The membrane velocity with respect to the velocity at the spreading edge at a distance R from the center is:

One-dimensional monolayer/single bilayer

$$v = \frac{dR}{dt} \quad (a)$$

One-dimensional double bilayer

$$v = 2 \frac{dR}{dt} \quad (b)$$

(13)

Eq. (12a) and (12b) can be inserted into Eq. (12), which leads to:

One-dimensional monolayer/single bilayer

$$\zeta \frac{dR}{dt} R = \sigma_s - \sigma_0 \quad (a)$$

One-dimensional double bilayer

$$\zeta 2 \frac{dR}{dt} R = \sigma_s - \sigma_0 \quad (b)$$

(14)

During spreading, the radius of the circular lipid patch would grow from R_0 (the reservoir radius) at time t_0 to $R(t)$ at time t . Integrating the left side of Eq. (13a) and (13b), from $R(0)$ to $R(t)$ and the right side of the equations from time $t=0$ to t gives:

One-dimensional monolayer/single bilayer

$$\zeta \frac{1}{2} R^2(t) = (\sigma_s - \sigma_0)t \quad (a)$$

One-dimensional double bilayer

$$\zeta R^2(t) = (\sigma_s - \sigma_0)t \quad (b)$$

(15)

The radius of the spread at $t = 0$ is $R(0) = 0$. Rearranging Eq. (14a) and (14b) gives:

One-dimensional monolayer/single bilayer

$$R(t) = \sqrt{\frac{2(\sigma_s - \sigma_0)t}{\zeta}} \quad (a)$$

One-dimensional double bilayer

$$R(t) = \sqrt{\frac{(\sigma_s - \sigma_0)t}{\zeta}} \quad (b)$$

(16)

The derivative of $R(t)$ in Eq. (15a) and (15b) with respect to t is the velocity of the membrane v :

One-dimensional monolayer/single bilayer

$$v = \frac{dR}{dt} = \sqrt{\frac{(\sigma_s - \sigma_0)}{2\zeta t}} \quad (a)$$

One-dimensional double bilayer

$$v = \frac{dR}{dt} = \sqrt{\frac{(\sigma_s - \sigma_0)}{4\zeta t}} \quad (b)$$

(17)

As mentioned above, the spreading power $S = \sigma_s - \sigma_0$ is the product of the spreading coefficient and the friction coefficient:

$$\beta = \frac{S}{2\zeta} \quad (6)$$

Inserting Eq. (6) into Eq. (16a) and (16b) will provide the spreading coefficient β for monolayer–single bilayer and double bilayer spreading, respectively.

One-dimensional monolayer/single bilayer

$$v = \sqrt{\frac{\beta}{t}} \quad (a)$$

One-dimensional double bilayer

$$\frac{v}{2} = v_R = \sqrt{\frac{\beta}{t}} \quad (b)$$

(18)

After determining the spreading coefficient with regards to membrane velocity by adapting a one-dimensional model, we will now determine the relationships for a two-dimensional model. The two-dimensional model would provide more insights for lipid self-spreading in correlation with experiments, since the two-dimensional wetting of a lipid membrane can be monitored experimentally, for example, via confocal microscopy (Figure 1d). In such experiments, a self-spreading membrane doped with a membrane-attached fluorophore can be observed from top view as a circular patch with quite a distinct circumference (Figure 1d). On this circular patch, we imagine an arbitrary ring with an inner radius r_1 and the outer radius r_2 (Figure 1). During the spreading of an incompressible membrane, the number of lipid molecules within this ring should be constant. The law of mass conservation would require the flux – rate of lipid flow per cross-sectional area – at distance r_1 (J_1) and r_2 (J_2) to be equal.

$$J_1 = J_2$$

The lipid molecules coming from the reservoir will pass through r_1 with velocity v_1 and subsequently r_2 with velocity v_2 :

$$2\pi r_1 \rho v_1 = 2\pi r_2 \rho v_2$$

where ρ is the particle density. Note that we had earlier assumed the membrane to be incompressible, thus ρ is constant. Therefore, $r v_r$ is constant. This means that the velocity v_r of the lipid molecules at any arbitrary circle with radius r can be related to the velocity v_R of the lipids at the spreading edge as following:

$$r v_r = R v_R \quad (19)$$

We will initiate the formulation of our two-dimensional model by rearranging Eq. (19): $v_r = \frac{R}{r} v_R$. As explained above, during the determination of the one-dimensional model, the dynamics of spreading monolayers-single bilayers and the double bilayers will be formulated separately due to the variations in the spreading edge velocity. We will use notation "a" for the equations defining the monolayers/single bilayers and "b" for the equations defining the double bilayers.

Two-dimensional monolayer and single bilayer

$$v_r = \frac{R}{r} \frac{dR}{dt} \quad (a) \quad (20)$$

Two-dimensional double bilayer

$$v_r = 2 \frac{R}{r} \frac{dR}{dt} \quad (b)$$

The velocity of the spreading edge of the double bilayer membrane is again half the velocity of the membrane (v_r). The radial tension gradient drives the spreading process and it is balanced by the frictional stress (Eq. 7):

$$\zeta \bar{v} = \nabla \sigma \Rightarrow \zeta v_r = \frac{d\sigma}{dr}$$

Inserting Eq. (19a) and (19b) into Eq. (8) gives:

Two-dimensional monolayer and single bilayer

$$\zeta v_r = \frac{R}{r} \frac{dR}{dt} = \frac{d\sigma}{dr} \quad (a) \quad (21)$$

Two-dimensional double bilayer

$$\zeta v_r = \frac{R}{r} \frac{dR}{dt} = 2 \frac{d\sigma}{dr} \quad (b)$$

Integrating Equations (20a) and (20b) from R_0 (the reservoir radius at time t_0) to R (the radius of the growing circular lipid film at time t) gives:

Two-dimensional monolayer and single bilayer

$$\zeta R \frac{dR}{dt} \ln\left(\frac{R}{R_0}\right) = \sigma_s - \sigma_0 \quad (a)$$

Two-dimensional double bilayer

$$2\zeta R \frac{dR}{dt} \ln\left(\frac{R}{R_0}\right) = \sigma_s - \sigma_0 \quad (b)$$

(22)

The spreading power ($S = \sigma_s - \sigma_0$) is the product of spreading coefficient and friction coefficient. Eq. (21a) and (21b) are therefore rearranged as following to obtain the two-dimensional spreading coefficients:

Two-dimensional monolayer and single bilayer

$$R \frac{dR}{dt} \ln\left(\frac{R}{R_0}\right) = \frac{\sigma_s - \sigma_0}{\zeta} = 2\beta \quad (a)$$

Two-dimensional double bilayer

$$R \frac{dR}{dt} \ln\left(\frac{R}{R_0}\right) = \frac{\sigma_s - \sigma_0}{2\zeta} = 2\beta \quad (b)$$

(23)

By monitoring the self-spreading of a fluorescently labelled monolayer on a SU-8 surface over time under a microscope, β has been calculated to be $1-3 \mu m^2/s$. [3] Note that SU-8 is a hydrophobic epoxy polymer that is commonly used as substrate, due to its favourable processing properties [3, 60]. In content of the same study, Eq. (22 a/b) have been solved numerically and shown to yield a good fit with the experimental data. The tension of the reservoir is considered to be on the order of the lysis tension of a single bilayer membrane ($6 \text{ mN} / m$). "Lysis" can be thought of as the process of breaking down a single bilayer. Since a multilamellar reservoir consists of several bilayers, monolayer spreading can only be initiated by the lysis of a single bilayer within the reservoir. The spreading power S is the difference in the adhesion energy at the membrane-SU-8 interface (σ_s) and the reservoir (σ_0): $\sigma_s - \sigma_0$. For simplicity, S has been assumed to be in the order of the reservoir tension. Taking $\beta \approx 3 \mu m^2/s$ and S as $6 \text{ mN} / m$, ζ for monolayers spreading on a SU-8 has been estimated to be $\sim 10^9 \text{ Pas} / m$. This value is comparable to the friction coefficients estimated between the monolayer leaflets within a bilayer ($\sim 10^8 - 10^9 \text{ Pas} / m$) [3, 65].

Rädler et al. have reported the experimental values of β for a sliding bilayer to be up to $43 \mu m^2/s$. [2] The high β values indicate a much faster spreading motion compared to the monolayers. This is predictable since the presence of the lubricating water layer (25 \AA) enhances the sliding by reducing friction.

The friction coefficient, which characterizes the lower monolayer leaflet of the distal bilayer and the upper monolayer leaflet of the proximal bilayer during bilayer rolling (double bilayer spreading), has been experimentally determined to be $5 \times 10^7 \text{ Pa}\cdot\text{s} / \text{m}$. [4] However, a spreading coefficient for double bilayers has not yet been revealed. This may be due to the relatively complicated spreading dynamics of double bilayer membranes. The few assumptions we have made above to develop a theoretical model for the calculation of spreading coefficients may not necessarily be fully satisfied for double bilayers. For example, we assumed that the tension of the reservoir was constant at all times during spreading. However, there is evidence confirming that the inter-bilayer defects naturally exist or spontaneously form in such reservoirs [42, 66]. In this case, the reservoir tension would be expected to vary, as it cannot be maintained. Similarly, Rädler et al. have reported ceasing of double bilayer self-spreading due to the exhaustion of the lipid source [2]. Another variable parameter during double bilayer spreading would be the thickness of the water layer, on which the distal bilayer slides. During the spreading of single bilayers, the inter-bilayer distance is regulated by the hydration forces and van der Waals interactions, as mentioned above. For a distal bilayer sliding on a proximal bilayer, no such forces apply. Additionally, surface roughness, irregularities or defects may cause the thickness of the water layer to alter, which would in turn influence the magnitude of friction.

4. Lipid membrane rupturing

In the previous sub-chapter, we described the details of the spreading motion of lipids on solid supports in various forms, without reporting on the eventual outcome of such spreading. Spreading continues until the reservoir is depleted, or exhausted due to defects. This will cause termination of lipid supply from the source to the spreading membrane, so that the spreading motion will slow down and eventually almost stop. In the meantime, the adhesion energy remains constant. This means that regardless of the insufficient lipid supply, the spreading edge of the membrane will favour lipid wetting and tend towards adhering. Note that a lipid membrane cannot stretch more than 5% of its surface area [67]. The fate of the spreading from this point on will differ depending on the type of the surface and corresponding spreading mode.

When the reservoir is completely consumed and the spreading velocity reaches zero, the circumference of a spreading monolayer starts to “evaporate” [68]. Evaporation occurs when the hydrophobic tails of individual lipids lay open and completely adhere to the substrate. If the membrane is tagged with fluorophores, the evaporating rim of the membrane can be observed as a fuzzy edge rather than a distinct one. The driving force for the evaporation of monolayers is the increase in entropy which in turn minimizes the Gibbs free energy.

Similarly, single bilayer spreading simply comes to an end when the reservoir is depleted. It has recently been shown that an additional stock of lipids can be provided to a supported bilayer lacking a reservoir, by using a microfluidic pipette device for continuous supply [10]. Briefly, at the tip of the microfluidic pipette, a virtual flow cell provides a steady hydrody-

namically confined flow, featuring a low Reynolds (Re) and a high Péclet (Pe) number. This flow cell can therefore deliver liquid cargo locally to a surface under highly controlled laminar flow conditions. By using the microfluidic pipette, it is possible to supply and fuse small unilamellar lipid reservoirs (vesicles ~ 100 nm) into an existing lipid bilayer patch. This can lead to interesting wetting behaviour. If the new supply of lipids are zwitterionic with a net charge of zero (e.g., POPC), no further effect in wetting is observed and the size of the bilayer lipid patch remains constant over time. If the lipid stock provided to the single bilayer patch consists of cationic transfection lipids (e.g., DOTAP), the single bilayer starts to further wet the substrate. This is possible due to the intercalation of DOTAP lipids into the membrane, which are exposed via the microfluidic pipette. By means of the microfluidic device, spreading of membranes can be precisely controlled, and patches of desired size and composition can be easily generated. This provides a means of prototyping supported membranes in a rapid and reproducible fashion.

For a double bilayer membrane, the free energy can further be minimized, if the distal bilayer ruptures and adheres on the substrate. Rupturing of the distal membrane is possible if the tension of the membrane increases due to the continuous adhesion of the membrane edge to the substrate, and exceeds the lysis tension. In 2010, two forms of ruptures occurring in the distal bilayer of spreading double bilayer membranes have been reported. The “floral” ruptures, named after pore morphologies resembling flowers, can be observed mostly at the centre of a circular lipid spread propagating towards its periphery (Figure 2a). Such pores continuously grow until the double bilayer membrane entirely transforms into a single bilayer membrane on the solid support. The second rupture type appears in “fractal” patterns, most frequently at the circumference of the lipid patch, and develops inwards in the form of avalanches (Figure 2b). Within the fractal ruptures there remain “islands”, the entrapped regions of the distal membrane which are strongly pinned to the proximal bilayer. Except for the islands, the lipid material of the upper bilayer migrates towards the edges (cf. Figure 1c) and is deposited on the surface in the same manner as during floral rupturing. Since the fractal ruptures propagate in form of avalanches, the wetted area on the surface increases step-wise over time. Both types of rupture formation are spontaneous, and occur when the lipid reservoir is exhausted. Discrimination among the two rupture types has been attributed to the amount of pinning between the two bilayers. The pinning can be established by means of Ca^{2+} or other multivalent cations present in the ambient buffer. A high number of pinning sites is assumed to favour fractal morphology. Precise control of the number and location of pinning sites during spreading/rupture experiments has not yet been achieved.

We want to dedicate this sub-chapter to membrane ruptures, as the displacement of the membrane on the surface during rupturing is a form of wetting of the solid substrate, and also a simultaneous form of de-wetting of the proximal bilayer membrane (Figure 2c). Next, we will describe a mathematical analogy between the dynamics of floral ruptures and the dynamics of flow in conventional “porous media”. A porous medium can be depicted as a fluidic compartment packed regularly with particles, for example, micron-size beads. Such fluidic media can consist of, for example, glycerol, oil, or water. If now a secondary fluid of lower viscosity is pushed through the porous medium to displace the existing fluid, a mor-

phologically instable interface between the two immiscible fluids is formed. Common injection fluids in flow experiments in porous media are water and air. Water can be injected only into liquids with higher viscosity, e.g., glycerol, but is often used as the main medium itself, if the injected fluid is air. The instability at the boundary of two immiscible fluids formed during the flow in a porous medium exhibits complex, finger-like patterns, therefore, is referred to as “viscous fingering” [69]. Membrane ruptures highly resemble these fingering instabilities. A membrane flow causing edge instabilities is comprehensible since the lipid membranes are considered as two-dimensional fluids. One interesting aspect regarding the similarities between the viscous fingering and the membrane pore edge instabilities is the difference in length scales: membrane ruptures are of micrometer size where fingering patterns is in the order of centimetres.

Viscous fingering instabilities can be observed in a “Hele-Shaw cell”, which is an experimental set up explicitly designed to simulate the flow in a three-dimensional porous media in a two-dimensional environment. The cell consists of two flat glass plates, positioned in parallel and separated with an infinitesimally small distance h . If h is very small, the flow inside the cell becomes incompressible ($\nabla \cdot \vec{v} = 0$). Eq. (7), which describes the force balance for spreading solid-supported membranes, is in fact mathematically identical to the Brinkman equation used to describe flow in porous media. Correspondingly, a characteristic length scale L_c , which can be determined from Eq. (7), is equivalent to the Brinkman length scale.

Eq. (7), which describes the membrane flow ($\zeta \vec{v} = \nabla \sigma$), is the same as the Hele-Shaw equation, a form of the Darcy equation specific to the Hele-Shaw flow. This flow can be expressed as:

$$\vec{v} = -\frac{h^2}{12\eta} \nabla P \quad (24)$$

where \vec{v} is the velocity field. This vector mathematically describes the motion of the fluid where the length of the vector field is the flow speed, h is the distance between the two plates, η is the viscosity of the fluid, and ∇P is the pressure gradient. η may depict the viscosity of the existing in the Hele-Shaw cell (η_1) or the subsequently introduced fluid (η_2).

The inviscid edge at the moving boundary of the fluids is balanced by the pressure of the invading liquid:

$$P = -\gamma_L c \quad (25)$$

where P is the pressure, γ_L is the surface tension of the boundary, and c is the edge curvature. If the viscosity of the injected fluid, such as air, is significantly lower than the viscosity of the accommodating liquid, e.g., water or oil. In practice, the fluid can be considered to be inviscid (zero viscosity). When a pore opens in the membrane, the water in the ambient buffer penetrates into the ruptured areas of the membrane. However, mainly the friction influences the flow dynamics of a supported membrane and the effect of water viscosity is considered to be

insignificant. Hence, the opening of a pore in the membrane is equivalent to air injection to a Hele-Shaw cell. At the boundary of a rupture, the membrane tension σ is balanced by the line tension γ :

$$\sigma = \gamma c \tag{26}$$

where c is the edge curvature of the rupture. The line tension emerges when lipids curve at any membrane edge to avoid the exposure of the hydrophobic fraction of the lipids to the aqueous environment.

The instability of a membrane pore edge, where the pore void represents an inviscid fluid, is mathematically analogous to a Saffman-Taylor instability [69]. A periodic membrane edge modulation can be expressed as $u = \varepsilon(t) \sin(qx)$, where for a wavelength of L , ε is the peak amplitude of the modulation. If Eq. (7) and (26) are solved with this boundary condition, where $\nabla \vec{v} = 0$, the resulting wavelength gives the dynamics picture equivalent to the Saffman-Taylor instability observed in a Hele-Shaw cell. The growth rate of an amplitude $\varepsilon(q)$ with wave number $q = \frac{2\pi}{L}$ therefore is:

$$\frac{\partial \varepsilon}{\partial t} = q \left(V - \frac{\gamma q^2}{\zeta} \right) \varepsilon \tag{27}$$

Here, γ is the edge tension of the pore which corresponds to γ_L . V is the mean velocity of the interface at the pore edge.

In a basic Hele-Shaw cell the porosity is regular. An inhomogeneous porosity can be introduced into the cell by placing grains, e.g., glass beads at random locations. This leads to irregular permeability where the capillary forces become significantly effective and eventually cause fractal displacements termed invasion percolation clusters. The percolation clusters form when invading fluid chooses the “path of least resistance”, entrapping islands of the displaced fluid. This can be achieved, for example, by injecting air into water. The displacements appear in characteristic bursts with a broad size distribution, known as Haines jumps, which are similar to the avalanches observed during fracturing of the lipid membranes. The islands within the clusters are comparable to the islands surrounded by the fractal ruptures. Another similarity is the fractal dimension (D) of the ruptures: 1.71. This is lower than the theoretically estimated dimension of a percolation cluster $D = 1.83$, but equal to typical experimental values (1.70–1.71) [70].

A Hele-Shaw cell contains particles or beads which provide the effect of porosity. In between the proximal and the distal membranes, there are no particles, but a corresponding effect is established by “pinning”. The pinning can be due to the Ca^{2+} ions which bridge bits of the two bilayers together [71]. The pinned regions become visible during formation of floral ruptures in forms of thin threads at the pore edges [4]. The pinning points, where the fluidity is reduced, act like solid particles and play the role of grains in a Hele-Shaw cell. One other reason for

pinning can be the surface structure. Nanometer-sized grains of silicon dioxide (SiO_2) are known to create incisions in solid-supported lipid membranes. The granules of surface therefore can punch through the proximal bilayer and act like particles placed in between the two bilayers. The flow of lipids during rupturing is therefore considered to be through a porous medium.

A clearly defined analogy between the fractal ruptures and the invasion percolation instabilities, as we have previously shown for the floral ruptures and the Saffman-Taylor instabilities, has not yet been established. However, it is possible to estimate a characteristic length scale for membrane pores, within which they are not expected to exhibit instabilities.

Free standing membranes produce circular pores with straight edges [72]. An unstable pore edge in such a membrane can be pictured as a wave or a modulation. The excess energy of an

instability compared to a straight edge ($u = 0$) over one wavelength is $E = \gamma \int_0^L dx \frac{1}{2} \left(\frac{du}{dx} \right)^2 = \pi^2 \gamma \frac{\varepsilon^2}{L}$.

The instable membrane pore edge will over time relax to a straight edge due to dissipation which emerges from the two-dimensional Stokes flow of surfactants in the membrane. This means we have to take into account the membrane viscosity (μ) regarding dissipation of the excess energy at a pore edge. The dissipation scales as $T\dot{S} \sim \mu L^2 \left(\frac{v}{L} \right)^2 \sim \mu V^2 \sim \mu \dot{\varepsilon}^2$. This has been obtained by integrating over one wavelength L , the second term of the dissipation function of spreading membranes (Eq. (32)), on which we will elaborate in the paragraphs further down.

Balancing the excess edge energy with dissipation ($T\dot{S} + \dot{E} = 0$) leads (on a scaling level) to $\dot{\varepsilon} \sim \frac{1}{\tau} \varepsilon$. Therefore, the relaxation time (τ) is:

$$\tau \sim \frac{\mu}{\gamma} L \quad (28)$$

In a supported membrane, τ is much longer and increases rapidly with the wavelength of the modulation: the dissipation due to sliding friction, over one wavelength L , scales as $T\dot{S} = \int dA \frac{1}{2} \zeta v^2 \sim \zeta L^2 \dot{\varepsilon}^2$, where ζ is the friction coefficient between the proximal and the distal bilayers.

Balancing the dissipation and the excess energy of the instability gives:

$$\tau \sim \frac{\zeta}{\gamma} L^3 \quad (29)$$

A rupture propagating at velocity v exposes a membrane edge length L in time $\tau = \frac{L}{v}$. By inserting τ into Eq. (29) gives a characteristic length (L_c):

$$L_c = \sqrt{\frac{\gamma}{\zeta v}} \quad (30)$$

For modulations larger than L_c , the ruptures will propagate before the edge shape modulation can possibly relax. v has been determined from experimental observations of fractal rupture [4] to be $20\text{--}30 \frac{\mu\text{m}}{\text{s}}$. Taking $\gamma \approx 10 \text{ pN}$ and $\zeta \sim 5 \times 10^7 \frac{\text{Pa}\cdot\text{s}}{\text{m}}$, [4] L_c is calculated as $0.1 \mu\text{m}$. Above this length, pore edge dynamics is too slow to secure a stable pore edge. The size of fractal ruptures is in the order of several tens of micrometers and is therefore in agreement with the prediction.

Biological cells can also spread their membrane material on solid supports, often in order to be able to migrate. In some instances, a 200-nm thick lamellipodial sheet protrudes from the cell body onto the substrate. [73] The sheet includes a double layer of plasma membrane in addition to actin filaments sandwiched in between the layers. The detailed mechanism of cellular wetting is a subject still under debate. Whether the proceeding edge is rolling or sliding driven by actin polymerization is not yet known. The lamellipodia-based cellular wetting, however, have been found to follow a similar power law as discussed in Section 1.3. [73] Spreading of cells can also be promoted by introducing trivalent ions to the substrate, for example, Eu^{3+} ions onto SiO_2 . [4] In such conditions, Chinese Hamster Ovary (CHO) cells continuously adhere onto the substrate. Interestingly, the adhesion leads to the formation of fractal ruptures [4] as well as the islands, in distal plasma membrane of spreading CHO cells. Upon rupturing, the wetted area on the substrate suddenly increases in a step-wise manner, similar to the fractal ruptures of the self-spreading double bilayers. The plasma membranes are connected to the underlying scaffolding layer (cytoskeleton) via linking molecules. The membrane flows around the linkers; the plasma membrane flow on cytoskeleton, therefore, can be considered as a two-dimensional porous media flow, i.e., Darcy flow. The tension causing the ruptures is still moderate and in the range of plasma membrane adhesion to the cytoskeleton, or membrane–membrane adhesion, suggesting that such ruptures can in fact occur in vivo.

Another form of lipid wetting on solid substrates involving ruptures is accommodated by inter-membrane “defects” or “fusion pores” (Figure 2d). The fusion pores are nanometer-sized circular conduits connecting two membranes in the shape of an hour-glass. The dimension of pores ($\sim \text{nm}$) makes direct observations with the current microscopy technologies tremendously challenging. An alternative way is to study the flow phenomena, indirectly, by the fluorescent intensity-based wetting area analysis of membranes. [42] In the following paragraphs, we will talk about double bilayer membranes, 1% of which consist of fluorescently tagged lipids. From the top view, such fluorescent distal membranes emit twice as intensely as the proximal membranes; therefore, the two bilayers can be easily distinguished.

The double bilayer membranes mentioned above exhibiting floral or fractal ruptures consists of two bilayers which are intact, performing a rolling motion. In some occasions, the proximal and distal bilayers split along the circumference. After splitting, the proximal bilayer continues

to wet the surface, which can be observed by increasing the wetted area on the substrate. The area of the distal bilayer membrane remains unchanged over the time period of a few minutes, followed by sudden decreases caused by instant avalanche ruptures. The decrease in the area of the distal bilayer simultaneously causes an increase in the wetted area by the proximal bilayer. This supports the notion of a physical connection among the two bilayers, through which the lipids are transferred. The outer border of the distal membrane does not expand along the peripheries upon rupturing, as occurs for the floral and fractal ruptures, indicating that the distal membrane is not dragged by the proximal membrane along the circumference. The stretching and eventual rupturing of the distal membrane can therefore be caused by the downwards lipid flow towards the proximal bilayer, most likely through narrow vertical channels. [42]

Defects among lipid membranes may have already formed during swelling of MLVs or form dynamically during spreading as a response to physical or chemical cues. We had briefly mentioned in Section 1.3 the defects existing in onion vesicles or MLVs. Since the lipid layers packed in the reservoir later spreads on the surface, these defects can be transferred to the supported membranes. Additionally, changes in membrane tension may cause instantaneous (\sim nanoseconds) formation of defects in membranes. Fusion is a thermally agitated process and alterations in line tension can promote the formation of fusion pores. Formation of defects can also be induced by the presence of multivalent ions, e.g., Ca^{2+} , in the ambient buffer. 2 mM of Ca^{2+} has been reported to advance the formation of defects among myelin sheaths of neurons, 80% of which consists of lipid material. The lipid transfer among the bilayers can as well be enhanced by hemi-fusion pores through which the dynamics change from bilayer sliding to monolayer sliding. As we had mentioned in Section 1.3, the sliding friction coefficient for monolayers is much higher than bilayers. Furthermore, the transformation of hemi-fusion to fusion pores is very energy-intensive and complex. For the simplicity of calculations, we will only assume defects to be in the shape of fusion pores in this section. We will discuss the monolayer sliding among the bilayers further in this section in another context.

The dynamics of lipid transfer via a fusion pore can be characterized semi-quantitatively via a “dissipation” function. Our model consists of a circular proximal bilayer, a circular distal bilayer and as an initial assumption: a single fusion pore with a diameter of 10 nm connecting these two membranes. Lipids flow from distal to proximal bilayer through the 10 nm defect, driven by the continuous adhesion of proximal bilayer to the substrate (Figure 2d). In this flow, there would be two separate forms of energy loss (dissipation). The first one is friction. The friction applies to the region (1) in between the proximal bilayer and the surface, (2) in between two bilayers since distal bilayer is de-wetting the proximal bilayer. The second form of dissipation is due to the viscous flow around the fusion pore. The lipid flow is expected to be different in remote areas of the membrane compared to the proximity of the pore. This is because the pore is small and the surfactants flowing through the pore collide with each other more intensely than they would in distant areas. Next, we will quantify and compare these two types of dissipations. If the magnitudes are compatible in relevant time scales, we will conclude that a single pore of 10 nm is sufficient to accommodate such a flow in between the

membranes. If viscous flow (Stokes flow) cause dissipation that is much stronger than the frictional, this will indicate that several pores are required.

This brings us back to Eq. (7), where the difference of frictional and viscous forces determines the tension gradient across the membrane. A characteristic length scale where the frictional forces are of the same order as the viscous forces can be obtained based on Eq. (7) as: $\zeta V \sim \mu \frac{V}{L^2}$. V is the characteristic velocity to determine the characteristic length scale. The cross-over length scale $L_c = \sqrt{\frac{\mu}{\zeta}}$ can help us to compare the viscous forces to the frictional forces. One can think of L_c as the “Reynolds number” of fluid mechanics, which is the ratio of inertial forces to viscous forces within a fluid. Low Reynolds numbers indicates laminar, high Reynolds numbers the turbulent flow. Similarly, above L_c the frictional forces are dominating membrane flow dynamics, whereas below L_c , the viscous forces are effective. In the following we will estimate L_c in order to be able to confirm that it is rational to take into account the viscosity, considering a membrane flow around a pore of 10 nm.

The friction coefficient is:

$$\zeta = \frac{\eta_w}{d_w} \tag{31}$$

where η_w is viscosity and d_w is the thickness of the water layer on which the bilayer is sliding. There may be two bilayers sliding on a water layer under the spreading conditions described above: the distal bilayer slides on the proximal and the proximal slides on the surface. If we take η_w as $8.9 \times 10^{-3} \text{ dyn s cm}^{-1}$ and d_w as 1 nm, we can determine L_c to be $\sim 30 \text{ nm}$. The thickness of the water layer between the bilayers can be slightly higher than the one between the surface and the proximal bilayer. With increasing d_w , the order of magnitude for L_c would not change. Above $L_c = 30 \text{ nm}$, the sliding friction dominates over viscosity. Since we assume the pore size to be $\sim 10 \text{ nm}$, it can be concluded that the pore vicinity will high likely be under the influence of the viscous forces.

For two-dimensional incompressible flow of the membrane, Eq. (7) leads to the following dissipation function [20]:

$$T\dot{S} = \int dA [\zeta \vec{v}^2 + 2\mu (\frac{\partial v_i}{\partial x_k} + \frac{\partial v_k}{\partial x_i})^2] \tag{32}$$

v_i, v_k are the components of velocity and x_k, x_i are the components of position, where i and k change from 1 to 2 in a two-dimensional membrane. We assume that the membrane flow is radially symmetric, where $v = \frac{r_p}{r} v_p$ around a pore with a membrane velocity of v_p in the pore

channel. Integrating Eq. (32) from the pore radius r_p to the radius of the distal membrane island patch R (Figure 2d) leads to:

$$T\dot{S} = 2\mu \int dr 2\pi r \left[\left(\frac{\partial v}{\partial r} \right)^2 + \left(\frac{v}{r} \right)^2 \right] = 8\pi\mu v_p^2 r_p^2 \int_{r_p}^R \frac{dr}{r^3} \approx 4\pi\mu v_p^2 \quad (33)$$

The integral Eq. (33) converges rapidly when R increases. This means that the viscous dissipation is intense in the pore area and is not as significantly effective in remote areas of the membrane. Taking into account the dissipation on both the proximal and the distal bilayer side of the pore, we obtain $T\dot{S} = 8\pi\mu v_p^2$, which is the total dissipation due to the viscous flow around a circular pore. The membrane viscosity μ is in the order of water viscosity ($\mu = \eta$ (water viscosity) $\times 1 \mu\text{m}$).

The dissipation caused by the sliding friction is composed of two parts: The sliding between the two bilayers (ζ) is expressed by the first term and the sliding of the proximal bilayer on the surface (ζ_s) by the second term of Eq. (34):

$$T\dot{S} = 2\pi\zeta (2v_p)^2 r_p^2 \ln\left(\frac{R}{r_p}\right) + 2\pi\zeta_s v_p^2 r_p^2 \ln\left(\frac{R_s}{r_p}\right) \quad (34)$$

R_s is the radius of the proximal bilayer (Figure 2d). Unlike viscous flow, the dissipation due to sliding friction is not local and depends logarithmically on the size of the membrane patch. ζ ($5 \times 10^5 \text{ Pa}\cdot\text{s}\cdot\text{m}^{-1}$) and ζ_s ($5 \times 10^7 \text{ Pa}\cdot\text{s}\cdot\text{m}^{-1}$) are not material constants and their values depend on the amount of water trapped between the bilayers, as well as on the degree of adhesion. Assuming $\zeta = 5 \times 10^5 \frac{\text{Pa}\cdot\text{s}}{\text{m}}$, $\zeta_s = 5 \times 10^7 \frac{\text{Pa}\cdot\text{s}}{\text{m}}$, $R_s = 100 \mu\text{m}$, $R = 10 \mu\text{m}$ and $r_p = 10 \text{ nm}$ the viscous dissipation around a 10 nm defect turns out to be spatially localized and high, but it is not expected to exceed the dissipation due to the sliding friction of the membrane. As a result, only a single pore can be sufficient to accommodate the rapid lipid transfer.

One can think of opening of large area pores in distal membranes as the process of de-wetting of the proximal bilayer. It is possible to reverse de-wetting by treating the pores with chemical 'repair' agents. When pores open in the membrane, the multivalent ions in the ambient buffer such as Ca^{2+} can penetrate through the pore edges and eventually pin fractions of the upper and lower bilayers together. At this instant, chelators such as 1,2-bis(o-aminophenoxy)ethane- N,N,N',N' -tetraacetic acid (BAPTA) can be introduced to the ambient buffer to target and deplete the Ca^{2+} ions. The chelators can bind to Ca^{2+} with high affinity and remove them from the pore edges and from the surface. This in turn frees the pore edges and reduces the overall membrane tension. Eventually, the membrane ruptures heal due to the pore edge tension (γ) and the distal membrane completely re-wets the proximal membrane. The lipid material

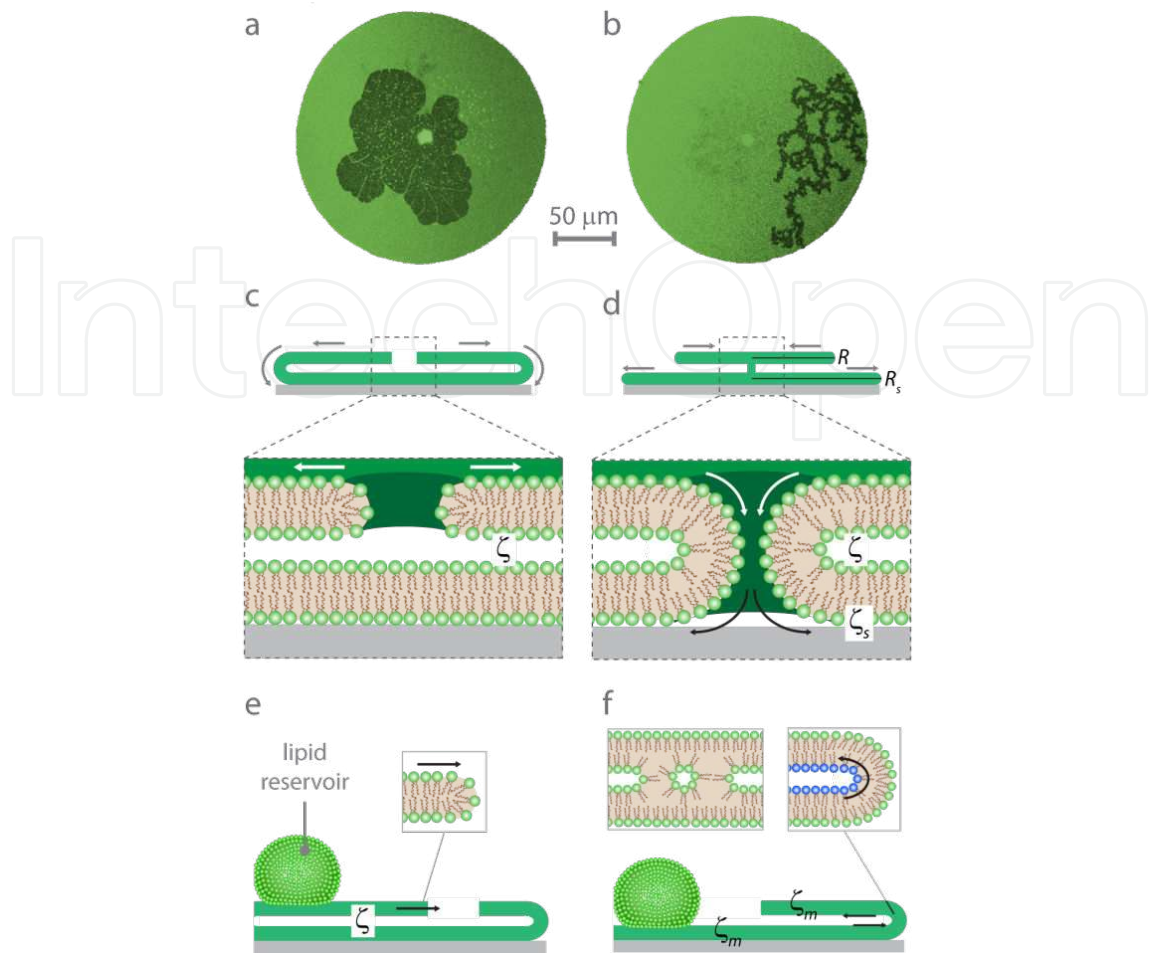


Figure 2. Biomembrane ruptures as a cause of wetting. Confocal fluorescence micrographs of (a) floral (b) fractal membrane ruptures (top view). The double bilayer membrane areas can be visualized as twice as intense as the single bilayer areas. Darker regions are the proximal membrane which is visible through the ruptures in the distal membrane. (c) Cross-sectional schematic view of a rupturing distal membrane, representing (a) or (b). (d) Cross-sectional schematic view of a fusion pore connecting proximal and distal bilayers. ζ and ζ_s are the friction coefficients which apply to the region between the bilayers and between the proximal bilayer and the surface, respectively. Pore/rupture repair via (e) bilayer sliding (f) monolayer sliding. In (e), there is a direct connection of the distal membrane to the lipid reservoir. In (f), the pore is around the reservoir which does not have any direct connection to the distal bilayer. The lipid transfer to the pore region can be via inter-monolayer sliding through the inverted micelle like defects (inset to the left) or simply by reverse sliding of the inner monolayer leaflet. The latter is represented by the inset to the right, in which the sliding monolayer is depicted in blue.

sealing the pores originates from the reservoir and re-locates around the pore area by means of two different mechanisms. In the following, we will explain these mechanisms in detail.

The large area pores can form at different locations in the distal membrane. A fraction of the ruptures appear towards the edges of the distal bilayer as we had described above (Figure 2 b,e). There, one side of the pore edge maintains a physical connection to the MLV through the distal bilayer. The sealing of pores becomes possible through “bilayer-on-bilayer sliding” from the reservoir towards the pore region. Alternatively, rupturing may occur around the MLV (Figure 2a,f). In this case, there remains no direct contact of the distal bilayer to the lipid

reservoir. The re-location of lipids towards the pore area can only be through the proximal bilayer. The free positive surface charges in the areas which are not wetted by the lipid membrane are mostly removed by BAPTA. This means depletion of fusogenic agents and termination of spreading. On the other hand, the access into the confined region between the proximal bilayer and the surface is impeded and chelation of the ions in the region above surface and underneath the membrane is expected to take significantly longer time. The total wetted area of the membrane on the solid substrate therefore can remain constant over several hours, confirmed by the experimental analysis [42]. While the edges of the spreading patch is pinned, reverse bilayer rolling becomes unlikely and one can presume the monolayer sliding to be the dominant flow mechanism for repair of such pores (Figure 2f).

To calculate the dissipation ($T\dot{S}$) during bilayer-on-bilayer sliding, we can neglect the second term in Eq. (32), and integrate the friction term from r_p to R_c . It is complicated to calculate dissipation regarding a pore at an arbitrary position in a circular spread since in that case the flow field would not be radial. Thus, we assume that the pore is centred, and consider R_c as the cut-off characteristic length scale. R_c is comparable to the size of the spread R_s . The integral will give $\pi\zeta r_p^2 \dot{r}_p^2 \ln\left(\frac{R_c}{r_p}\right)$, where ζ is the sliding friction coefficient between the distal and the proximal bilayers, v is the velocity of the sliding distal bilayer.

The dissipation ($T\dot{S}$) caused by the bilayer-on-bilayer sliding friction will be balanced by the edge tension energy \dot{E} of the pore: ($2\pi\gamma\dot{r}_p$) [74]:

$$\zeta r_p^2 \dot{r}_p^2 \ln\left(\frac{R_c}{r_p}\right) = -2\gamma \dot{r}_p \quad (35)$$

where $\dot{r}_p = \frac{dr_p}{dt}$. Integrating the left side of Eq. (35) from R_p (pore radius at $t = 0$, i.e., initial pore radius) to $r_p = 0$ (when the pore is closed), and the right side of the equation from 0 to τ (the time required to relax the pore) leads to:

$$\tau = \frac{\zeta R_p^3}{\gamma} \cdot \frac{1}{6} \left[\ln\left(\frac{R_s}{R_p}\right) + \frac{1}{3} \right] \sim \frac{\zeta R_p^3}{\gamma} \quad (36)$$

The radius of the proximal membrane R_s in Eq. (36) is only a logarithmic factor. This means that the size of the membrane spread on the surface does not determine the pore relaxation time and τ is rather highly depending on the initial pore size R_p . Note that Eq. (36) is a different form of Eq. (29) and can therefore be used to describe pores in cell membranes.

Now we will calculate the dissipation for the second scenario, where the membrane flow towards the pore area is through the monolayer sliding. The monolayer sliding occurs between

the two leaflets within a bilayer and will be opposed by friction. The friction coefficient (ζ_m) can be calculated by rearranging the first term of Eq. (32) as below:

$$T\dot{S} = \int_I dA \frac{1}{2} \zeta_m v_I^2 + \int_{II} dA \frac{1}{2} \zeta_m v_{II}^2 \quad (37)$$

Here, index I refers to the surface area of the proximal bilayer; index II of the distal bilayer. v is the velocity of the sliding monolayer. Integrating the first term of Eq. (37) from R_L (effective radius of the lipid source, $R_L \sim R_0$) to R_S (radius of the spread) and the second term from r_p (pore radius) to R_S gives:

$$T\dot{S} = 4\pi\zeta_m r_p^2 \dot{r}_p^2 \ln\left(\frac{R_S^2}{R_L r_p}\right) \quad (38)$$

where $\dot{r}_p = \frac{dr_p}{dt}$. Balancing Eq. (38) with the line tension energy of the pore ($T\dot{S} = \dot{E}$) gives

$$2 \frac{\zeta_m r_p^2}{\gamma} \dot{r}_p \ln\left(\frac{R_S^2}{R_L r_p}\right) = 1 \quad (39)$$

Based on experimental values inserted into Eq. (39), ζ_m has been calculated to be 10^5 to $10^6 \frac{Ns}{m}$. This friction coefficient is at least two orders of magnitude lower than typical values reported in the literature: 10^8 to $10^9 \frac{Ns}{m}$ [3, 65]. This means that a possible inter-leaflet monolayer sliding in the experimental conditions described above is occurring at much faster speed. Even though unlikely circumstances where a monolayer can slide under such rates have been previously simulated [75], alternatively, the “hemi-fusion pores” or stalks can accommodate the relocation of surfactants via monolayer sliding. One can think of hemi-fusion pores as intermediate forms of fusion pores where the two merged bilayers are continuous but have not yet evolved into an aqueous connection. A portion of pore closure mechanisms based on monolayer sliding can be assisted by hemi-fusion pores or defects resembling inverted-micelles (Figure 2f). Monolayer sliding in some areas may also be complemented by bilayer sliding which can explain the relatively low sliding frictions observed.

5. Summary

Research on model membranes has been conducted for decades, and the understanding of the dynamics of lipid films has reached advanced levels. However, enabled by the rapid advances in micro- and nano-technologies and analytical capabilities, new phenomena are frequently discovered, such as the occurrence of the fractal membrane ruptures in double bilayer membranes, which created a new, exciting link between solid materials and the biological soft matter world. The discovery of this rupture phenomenon was closely related to the spontaneous wetting of high-energy surfaces, which was experimentally established in a microen-

vironment under the microscope. This and the other wetting phenomena described in the previous sub-chapters are feature-rich and have possible implications not only for future technological advancements, such as membrane protein studies, cell migration, but also for very advanced applications such as chemistry confined to two dimension. The double bilayer, which was at the heart of these investigations, can be easily classified as a new membrane model, which adds to the mono-, bi-, and cushioned bilayers. One can perhaps also view it, on one hand, as a self-cushioning bilayer, but on the other hand, it is essentially a flat giant unilamellar vesicle, with an approximately 10 nm thin water layer encapsulated between the two bilayer sheets. The thus encapsulated volume is on the order of a few hundred femtoliters. It bears a richness in possibilities for application in nanofluidics and artificial cell models, and potentially allows through its spreading and rupturing dynamics greater insights into, for example, the membrane-related mechanisms of cell migration and chemotaxis. We have provided in this chapter an overview over the wetting and rupturing properties and features of phospholipid monolayers and double bilayers on solid support, which should provide the foundation for the design of new experiments, and in many cases the prediction of their outcome. The dynamics of pores in membranes and associated materials transport phenomena, which are also accompanied with wetting phenomena, are also discussed. There are some particular points where further research is required. For example, attempts to establish a relationship for the spreading coefficient to quantitatively describe the spreading dynamics of double bilayers have so far been unsuccessful, which leaves the spreading approach to lipid film formation in this case still not entirely predictable.

Author details

Irep Gözen¹, Paul Dommersnes² and Aldo Jesorka^{3*}

*Address all correspondence to: aldo@chalmers.se

1 Department of Engineering, Harvard University, Harvard School of Engineering and Applied Sciences, Pierce Hall, Cambridge, MA, USA

2 Department of Physics, Norwegian University of Science and Technology, Trondheim, Norway

3 Biophysical Technology Laboratory, Department of Chemistry and Chemical Engineering, Chalmers University of Technology, Göteborg, Sweden

References

- [1] Czolkos I, Jesorka A, Orwar O. Molecular phospholipid films on solid supports. *Soft Matter* 2011;7 (11):4562.

- [2] Radler J, Strey H, Sackmann E. Phenomenology and kinetics of lipid bilayer spreading on hydrophilic surfaces. *Langmuir* 1995;11 (12):4539.
- [3] Czolkos I, Erkan Y, Dommersnes P, et al. Controlled formation and mixing of two-dimensional fluids. *Nano Letters* 2007;7 (7):1980.
- [4] Gozen I, Dommersnes P, Czolkos I, et al. Fractal avalanche ruptures in biological membranes. *Nature Materials* 2010;9 (12):908.
- [5] van Meer G, Voelker DR, Feigenson GW. Membrane lipids: where they are and how they behave. *Nature Reviews Molecular Cell Biology* 2008;9 (2):112.
- [6] Bloom M, Evans E, Mouritsen OG. Physical properties of the fluid lipid-bilayer component of cell membranes - a perspective. *Quarterly Reviews of Biophysics* 1991;24 (3):293.
- [7] Pomorski TG, Nylander T, Cardenas M. Model cell membranes: Discerning lipid and protein contributions in shaping the cell. *Advances in Colloid and Interface Science* 2014;205:207.
- [8] Sackmann E. Supported membranes: Scientific and practical applications. *Science* 1996;271 (5245):43.
- [9] Walde P, Ichikawa S. Enzymes inside lipid vesicles: preparation, reactivity and applications. *Biomolecular Engineering* 2001;18 (4):143.
- [10] Ainla A, Gozen I, Hakonen B, et al. Lab on a Biomembrane: Rapid prototyping and manipulation of 2D fluidic lipid bilayer circuits. *Scientific Reports* 2013;3:2743.
- [11] Lobovkina T, Gozen I, Erkan Y, et al. Protrusive growth and periodic contractile motion in surface-adhered vesicles induced by Ca²⁺-gradients. *Soft Matter* 2010;6 (2): 268.
- [12] Reimhult E, Kasemo B, Höök F. Rupture pathway of phosphatidylcholine liposomes on silicon dioxide. *International Journal of Molecular Sciences* 2009;10 (4):1683.
- [13] Jesorka A, Stepanyants N, Zhang H, et al. Generation of phospholipid vesicle-nanotube networks and transport of molecules therein. *Nature Protocols* 2011;6 (6):791.
- [14] Ainla A, Jeffries GDM, Brune R, et al. A multifunctional pipette. *Lab on a Chip* 2012;12 (7):1255-61.
- [15] Thiam AR, Farese Jr RV, Walther TC. The biophysics and cell biology of lipid droplets. *Nature Reviews Molecular Cell Biology* 2013;14 (13):775.
- [16] Li J, Han D, Zhao Y-P. Kinetic behaviour of the cells touching substrate: the interfacial stiffness guides cell spreading. *Sci Rep* 2014;4:3910.
- [17] Czolkos I, Hakonen B, Orwar O, et al. High-resolution micropatterned Teflon AF substrates for biocompatible nanofluidic devices. *Langmuir* 2012;28 (6):3200.

- [18] Erkan Y, Halma K, Czolkos I, et al. Controlled release of chol-TEG-DNA from nano- and micropatterned SU-8 surfaces by a spreading lipid film. *Nano Letters* 2008;8 (1): 227.
- [19] de Gennes PG. Wetting: statics and dynamics. *Reviews of Modern Physics* 1985;57 (3):827.
- [20] Evans E, Sackmann E. Translational and rotational drag coefficients for a disk moving in a liquid membrane associated with a rigid substrate. *Journal of Fluid Mechanics* 1988;194:553.
- [21] Kochev V, Karabaliev M. Wetting films of lipids in the development of sensitive interfaces. An electrochemical approach. *Advances in Colloid and Interface Science* 2004;107 (1):9.
- [22] Suzuki K, Masuhara H. Growth of giant membrane lobes mechanically driven by wetting fronts of phospholipid membranes at water-solid interfaces. *Langmuir* 2005;21 (2):537.
- [23] Borghi N, Alias K, de Gennes PG, et al. Wetting fibers with liposomes. *Journal of Colloid and Interface Science* 2005;285 (1):61.
- [24] Richter RP, Brisson AR. Following the formation of supported lipid bilayers on Mica: A study combining AFM, QCM-D, and ellipsometry. *Biophysical Journal* 2005;88 (5): 3422.
- [25] Richter RP, Lai Kee Him J, Tessier B, et al. On the kinetics of adsorption and two-dimensional self-assembly of annexin A5 on supported lipid bilayers. *Biophysical Journal* 2005;89 (5):3372.
- [26] Richter RP, Bérat R, Brisson AR. Formation of solid-supported lipid bilayers: An integrated view. *Langmuir* 2006;22 (9):3497.
- [27] Furukawa K, Sumitomo K, Nakashima H, et al. Supported lipid bilayer self-spreading on a nanostructured silicon surface. *Langmuir* 2007;23 (2):367.
- [28] Erkan Y, Czolkos I, Jesorka A, et al. Direct immobilization of cholesteryl-TEG-modified oligonucleotides onto hydrophobic SU-8 surfaces. *Langmuir* 2007;23 (11):5259.
- [29] Zhou X, Moran-Mirabal JM, Craighead HG, et al. Supported lipid bilayer/carbon nanotube hybrids. *Nat Nano* 2007;2 (3):185.
- [30] van Meer G, Voelker DR, Feigenson GW. Membrane lipids: where they are and how they behave. *Nature Reviews Molecular Cell Biology* 2008;9 (2):112.
- [31] Gauthier NC. Plasma membrane area increases with spread area by exocytosis of GPI anchored protein compartment. *Biophysical Journal*;96 (3):151a.

- [32] Cho N-J, Frank CW, Kasemo B, et al. Quartz crystal microbalance with dissipation monitoring of supported lipid bilayers on various substrates. *Nature Protocols* 2010;5 (6):1096.
- [33] Gołabek M, Hołysz L. Changes in wetting and energetic properties of glass caused by deposition of different lipid layers. *Applied Surface Science* 2010;256 (18):5463.
- [34] Han X, Achalkumar AS, Cheetham MR, et al. A self-assembly route for double bilayer lipid membrane formation. *ChemPhysChem* 2010;11 (3):569.
- [35] Isono T, Ikeda T, Ogino T. Evolution of supported planar lipid bilayers on step-controlled sapphire surfaces. *Langmuir* 2010;26 (13):9607.
- [36] Oliver AE, Parikh AN. Templating membrane assembly, structure, and dynamics using engineered interfaces. *Biochimica et Biophysica Acta (BBA) - Biomembranes* 2010;1798 (4):839.
- [37] Gozen I, Billerit C, Dommersnes P, et al. Calcium-ion-controlled nanoparticle-induced tubulation in supported flat phospholipid vesicles. *Soft Matter* 2011;7 (21):9706.
- [38] Nabika H, Oowada M, Murakoshi K. Control of dynamics and molecular distribution in a self-spreading lipid bilayer using surface-modified metal nanoarchitectures. *Physical Chemistry Chemical Physics* 2011;13 (14):5561.
- [39] Nair PM, Salaita K, Petit RS, et al. Using patterned supported lipid membranes to investigate the role of receptor organization in intercellular signaling. *Nature Protocols* 2011;6 (4):523.
- [40] Mohamad S, Noël O, Buraud J-L, et al. Mechanism of lipid nanodrop spreading in a case of asymmetric wetting. *Physical Review Letters* 2012;109 (25):248108.
- [41] Gözen I, Jesorka A. Instrumental methods to characterize molecular phospholipid films on solid supports. *Analytical Chemistry* 2012;84 (2):822.
- [42] Gozen I, Dommersnes P, Orwar O, et al. Evidence for membrane flow through pores in stacked phospholipid membranes. *Soft Matter* 2012;8 (24):6220.
- [43] Gauthier NC, Masters TA, Sheetz MP. Mechanical feedback between membrane tension and dynamics. *Trends in Cell Biology* 2012;22 (11):527.
- [44] Subramaniam AB, Guidotti G, Manoharan VN, et al. Glycans pattern the phase behaviour of lipid membranes. *Nature Materials* 2013;12 (2):128.
- [45] Hirtz M, Oikonomou A, Georgiou T, et al. Multiplexed biomimetic lipid membranes on graphene by dip-pen nanolithography. *Nature Communications* 2013;4:2591.
- [46] Gozen I, Ortmen B, Poldsalu I, et al. Repair of large area pores in supported double bilayers. *Soft Matter* 2013;9 (11):2787.

- [47] Pietuch A, Janshoff A. *Mechanics of spreading cells probed by atomic force microscopy*, 2013;3 (7):130084.
- [48] Nguyen PA, Groen AC, Loose M, et al. Spatial organization of cytokinesis signaling reconstituted in a cell-free system. *Science* 2014;346 (6206):244.
- [49] Motegi T, Nabika H, Fu Y, et al. Effective brownian ratchet separation by a combination of molecular filtering and a self-spreading lipid bilayer system. *Langmuir* 2014;30 (26):7496.
- [50] Watanabe R, Soga N, Fujita D, et al. Arrayed lipid bilayer chambers allow single-molecule analysis of membrane transporter activity. *Nature Communications* 2014;5:4519.
- [51] Tabaei SR, Choi J-H, Haw Zan G, et al. Solvent-assisted lipid bilayer formation on silicon dioxide and gold. *Langmuir* 2014;30 (35):10363.
- [52] Shaali M, Lara-Avila S, Dommersnes P, et al. Nanopatterning of mobile lipid monolayers on electron-beam-sculpted Teflon AF surfaces. *ACS Nano* 2015;9 (2):1271.
- [53] Ma L, Li Y, Peng J, et al. Discovery of the migrasome, an organelle mediating release of cytoplasmic contents during cell migration. *Cell Research* 2015;25 (1):24.
- [54] Wu IL, Narayan K, Castaing J-P, et al. A versatile nano display platform from bacterial spore coat proteins. *Nature Communications* 2015;6:7548.
- [55] Shuttleworth R. The surface tension of solids. *Proceedings of the Physical Society of London Section A* 1950;63 (365):444.
- [56] Zhai L, Berg MC, Cebeci FC, et al. Patterned superhydrophobic surfaces: Toward a synthetic mimic of the Namib Desert beetle. *Nano Letters* 2006;6 (6):1213.
- [57] Sedev R, Fabretto M, Ralston J. Wettability and surface energetics of rough fluoropolymer surfaces. *Journal of Adhesion* 2004;80 (6):497.
- [58] Degennes PG. Wetting: statics and dynamics. *Reviews of Modern Physics* 1985;57 (3):827.
- [59] Dorrer C, Ruehe J. Some thoughts on superhydrophobic wetting. *Soft Matter* 2009;5 (1):51.
- [60] Czolkos I. Micro- and nano-scale devices for controlling two-dimensional chemistry. PhD Thesis, Chalmers University of Technology, 2009.
- [61] Chenevier P, Grandjean C, Loing E, et al. Grafting of synthetic mannose receptor-ligands onto onion vectors for human dendritic cells targeting. *Chemical Communications* 2002 (21):2446.
- [62] Israelachvili JN. *Intermolecular and surface forces*. 3 ed: Elsevier, 2011.

- [63] Yokota K, Toyoki A, Yamazaki K, et al. Behavior of raft-like domain in stacked structures of ternary lipid bilayers prepared by self-spreading method. *Japanese Journal of Applied Physics* 2014;53 (5):05FA11.
- [64] Evans EA, Hochmuth RM. Membrane viscoelasticity. *Biophysical Journal* 1976;16 (1):1.
- [65] Shkulipa SA, den Otter WK, Briels WJ. Thermal undulations of lipid bilayers relax by intermonolayer friction at submicrometer length scales. *Physical Review Letters* 2006;96 (18):178302.
- [66] Leng J, Nallet F, Roux D. Swelling kinetics of a compressed lamellar phase. *European Physical Journal E* 2001;4 (1):77.
- [67] Rawicz W, Olbrich KC, McIntosh T, et al. Effect of chain length and unsaturation on elasticity of lipid bilayers. *Biophysical Journal* 2000;79 (1):328.
- [68] Czolkos I, Guan J, Orwar O, et al. Flow control of thermotropic lipid monolayers. *Soft Matter* 2011;7 (16):6926.
- [69] Homsy GM. Viscous fingering in porous-media. *Annual Review of Fluid Mechanics* 1987;19:271.
- [70] Crandall D, Ahmadi G, Ferer M, et al. Distribution and occurrence of localized-bursts in two-phase flow through porous media. *Physica a-Statistical Mechanics and Its Applications* 2009;388 (5):574.
- [71] Akashi K, Miyata H, Itoh H, et al. Formation of giant liposomes promoted by divalent cations: Critical role of electrostatic repulsion. *Biophysical Journal* 1998;74 (6):2973.
- [72] Zhelev DV, Needham D. Tension-stabilized pores in giant vesicles - Determination of pore size and pore line tension. *Biochimica Et Biophysica Acta* 1993;1147 (1):89.
- [73] Dobereiner HG, Dubin-Thaler B, Giannone G, et al. Dynamic phase transitions in cell spreading. *Physical Review Letters* 2004;93 (11):108105.
- [74] Gozen I, Dommersnes P. Pore dynamics in lipid membranes. *European Physical Journal-Special Topics* 2014;223 (10):1813.
- [75] den Otter WK, Shkulipa SA. Intermonolayer friction and surface shear viscosity of lipid bilayer membranes. *Biophysical Journal* 2007;93 (2):423.

